Performance evaluation of solar hybrid combined cooling, heating and power systems: a multi-objective arithmetic optimization algorithm

Authors

Ling-Ling Li

- State Key Laboratory of Reliability and Intelligence of Electrical Equipment, Hebei University of Technology, Tianjin 300401, China
- Key Laboratory of Electromagnetic Field and Electrical Apparatus Reliability of Hebei Province, Hebei University of Technology, Tianjin 300401, China

E-mail: lilinglinglaoshi@126.com; lilingling@hebut.edu.cn

Xin-Yu Ren

- State Key Laboratory of Reliability and Intelligence of Electrical Equipment, Hebei University of Technology, Tianjin 300401, China
- Key Laboratory of Electromagnetic Field and Electrical Apparatus Reliability of Hebei Province, Hebei University of Technology, Tianjin 300401, China

E-mail: renxinyu0817@126.com

Ming-Lang Tseng * (Corresponding author)

- Institute of Innovation and Circular Economy, Asia University, Taiwan
- Department of Medical Research, China Medical University Hospital, China Medical University, Taichung, Taiwan

*E-mail: tsengminglang@gmail.com; tsengminglang@asia.edu.tw

Ding-Shan Wu

- State Key Laboratory of Reliability and Intelligence of Electrical Equipment, Hebei University of Technology, Tianjin 300401, China
- Key Laboratory of Electromagnetic Field and Electrical Apparatus Reliability of Hebei Province, Hebei University of Technology, Tianjin 300401, China

E-mail: 202121401066@stu.hebut.edu.cn

Ming K. Lim

- Adam Smith Business School, University of Glasgow, United Kingdom

Email: Ming.Lim@glasgow.ac.uk

Performance evaluation of solar hybrid combined cooling, heating and power systems: a multi-objective arithmetic optimization algorithm

Abstract

The coupling of solar thermal and photovoltaic technologies with combined cooling, heating and power systems has significant impacts on the reduction of fossil fuel consumption and pollutant emissions. In this study, a mathematical model of a hybrid combined cooling, heating, and power system consisting of thermal storage units, batteries, microturbines, photovoltaic units, and solar thermal collectors, is developed. Meanwhile, based on the following thermal load strategy and following electric load strategy, the following the state of battery strategy is proposed. A multi-objective arithmetic optimization algorithm is proposed by using non-dominated sorting, mutation operations, and external archive mechanism to optimize the configuration of the hybrid system under different strategies. Besides, an optimal compromise is obtained by technique for order preference by similarity to an ideal solution method. A large hotel case is used to evaluate the performance of the hybrid system under different strategies. The optimization results show that the Pareto solutions obtained by the developed optimization algorithm are uniformly distributed. Moreover, compared with the hybrid system under the following electric load and following thermal load strategies, the hybrid system under the proposed strategy achieves better primary energy saving ratio, carbon dioxide emission reduction ratio, and energy efficiency, and these indicators reach 46.56%, 54.64%, and 78.51%, respectively.

Keywords: solar thermal collectors; multi-objective arithmetic optimization algorithm; hybrid combined cooling, heating and power system; following the state of battery strategy

Nomenclature		BESR	boiler energy saving ratio
		η_{CCHP}	energy efficiency of CCHP system
Abbreviations		*Symbols*	
CCHP	combined cooling heating and power	E	Electricity
SP	separate production system	C	Cooling
FEL	following the electric load	Q	Heating
FTL	following the thermal load	F	Fuel
FB	follow the state of the battery	G	solar radiation
FHL	following a hybrid electric-thermal load	T	temperature
FEL-ECR	following electric load with electric cooling ratio	V	installation capacity
AOA	arithmetic optimization algorithm	η	efficiency
MOAOA	multi-objective arithmetic optimization algorithm	PC	performance coefficient
MOPSO	Multi-objective particle swarm optimization algorithm	f	objective function

MOEA/D	Multi-objective evolutionary algorithm based on decomposition		
TOPSIS	technique for order preference by similarity to an ideal solution	Subscripts	
PV	micro turbine		
ST	solar thermal	*bat*	battery
MT	micro turbine	*he*	heat exchanger
TES	thermal energy storage	*ac*	absorption chiller
CSR	cost saving ratio	*ec*	electric chiller
PESR	primary energy saving ratio	*HR*	heating recovery
CDERR	carbon dioxide emission reduction ratio	*GB*	gas boiler

Performance evaluation of solar hybrid combined cooling, heating and power systems: a multi-objective arithmetic optimization algorithm

1. Introduction

Nowadays, due to population growth, the problems of fossil fuel depletion, global warming, and increasing energy demand are becoming increasingly serious [1]. The exploitation of renewable energy sources is an important weapon to deal with these critical issues. In addition, improving the performance of energy systems is another way to achieve sustainability [2]. As one of the affordable and accessible renewable energy technologies, solar energy is effective to confront the high consumption of fossil fuels and substitute conventional energy sources [3]. Solar radiation is characterized by its high availability and its ability to be converted into useful electrical or thermal energy [4]. As energy-efficient, low-carbon, and clean modern systems, combined cooling, heating and power (CCHP) systems have been widely recognized as effective solutions in terms of addressing and solving the environmental pollution and resource crisis [5]. Accordingly, the combination of the fossil fuel-based CCHP system with the solar energy system is considered by some researchers to be an optimal way to produce many valuable outputs with high efficiency and clean energy [6]. On the one hand, solar technologies can reduce the consumption of fossil energy. On the other hand, the CCHP technologies improve reliability and efficiency [7]. However, due to a large number of constraints and variables in the combined supply system and the relative complexity of the operating strategy [8], the coupling of solar technology with the CCHP system inevitably has impacts on the optimization difficulty and operating strategy. However, many studies on solar hybrid CCHP systems are not comprehensive. In addition to design optimization, operational strategy optimization plays an important role in system performance. Accordingly, in this study, a new operation strategy is proposed for hybrid CCHP systems, and a new method is developed to solve the problem of optimal configuration of hybrid CCHP systems.

2. Literature review

The coupling of conventional CCHP systems with solar thermal (ST) collectors and solar PV panels has been explored by some researchers. Ai et al. [9] presented a novel CCHP system that combines a regenerative organic flash cycle (OFC) system with a solar thermal input system, through comparison with conventional CCHP systems, the primary energy ratio and external energy efficiency of the novel system reached 53.1% and 38.7%, respectively. Nami et al. [10] constructed a solar-assisted biomass trigeneration system, including concentrated solar collectors, and investigated the effects of summer/winter conditions and some decision parameters on system performance from sustainability and thermodynamic perspective. The results revealed that the designed system can provide 1 MWe of electricity, 55.35 kW of chilled water for space cooling, and 1241 kW of space heating. Han et al. [11] optimized the solar water heater area ratio as a free variable in a novel full-spectrum solar-assisted methanol CCHP system in a hybrid solar installation, aiming to improve the combined environmental, economic, and energy performance. The optimization results showed the best overall performance for a solar water heater area ratio of 0.5. The energy efficiencies and annual energy are improved by 17.3 % and 15.9 %, respectively. The carbon dioxide emissions are reduced by 70.6 %, the primary energy is saved by 22.6 %, and the total product cost per unit of energy is increased by 49.0 %. Mehregan et al. [12] presented a novel trigeneration system driven by flat-plate solar collectors and gas engines and investigated the performance of a building in terms of economic, environmental, and energy aspects. The performance of the system is analyzed by varying the capacity of the solar panels under four different scenarios, and the results indicated that using solar flat plate collectors and gas engines to meet demand is a suitable solution without the need for an auxiliary boiler.

The devices in a CCHP system focus on energy conversion, while the operational strategy focuses on managing the flow of energy between devices. Therefore, as one of the factors influencing a good design of CCHP systems, the operating strategy can achieve the management of the energy output and affect the system performance [57]. Huang et al. [13] aimed to address the problem of frequent partial-load operation caused by fluctuations in customer demand by comparing three different operating strategies, namely turbine inlet temperature, inlet air throttling, and inlet guide vanes and employing them to modify the characteristics of the gas turbine to promote the energy-saving performance of the combined cooling and power system at partial load. The key results indicated that the inlet deflector blade operation strategy is the best choice for the system. According to the energy output characteristics of the solar hybrid CCHP system. Yang et al. [14] adapted the operation strategy of the conventional CCHP system according to the energy output characteristics of the solar hybrid CCHP system and applied it to the solar hybrid CCHP system. The results show illustrated that the hybrid CCHP system in following electric load with electric cooling ratio (FEL-ECR) strategy is the best choice. The annual total cost saving ratio (ATCSR), CO_2 emission reduction ratio (CDERR), and primary energy saving ratio (PESR) of the system under this strategy reached 4.16%, 53.73%, 36.15%, respectively. Based on the minimum distance between the building load point and the system power output curve, Zheng et al. [15] proposed a new operating strategy, and compared it with the following hybrid electric-thermal load (FHL), following thermal load (FTL) and following electric load (FEL) strategies. It made the CCHP system match performance to be improved. The optimization results suggested that the novel strategy enabled the CCHP system matching performance to be improved. Li et al. [16] came up with hybrid FTL and hybrid FEL based on FTL and FEL and verified that the proposed strategy improves the energy and environmental performance of the system. However, the above strategies do not take the state of the energy storage devices in the system into account, which may cause excess energy to be wasted when the energy storage devices are full.

The optimization configuration of the CCHP system is commonly a complicated multidimensional optimization issue with a variety of objective functions and non-negligible constraints. Although the optimization methods for energy systems configuration are many and generally be divided into two categories: (1) metaheuristics, such as particle swarm optimization algorithm [17, 18], moth-flame optimization algorithm [19], tunicate swarm algorithm [20] and genetic algorithm [21-25]; and (2) mathematical planning, including linear planning [26, 27], nonlinear planning [28, 29], and dynamic planning [30, 31]. Compared with mathematical planning, metaheuristics can obtain the optimal solution quickly even if the optimal problem is complex. There are no restrictions on the use of metaheuristics, whereas mathematical planning has limitations such as convexity, nonlinearity, and linearity [32]. Wang et al. [33] used a genetic algorithm to optimize a multi-objective model of a hybrid CCHP system incorporating flexibility to obtain a Pareto front that takes a less degraded performance and a larger operational flexibility solution into account. The optimization results demonstrated a 438.9% increase in potential regulation ability and a 3.6% reduction in net interaction with the grid and grid connection levels. However, the increase in flexibility reduces the economic, environmental, and energy benefits achieved by the CCHP system by 3.0%, 56.4%, and 5.1%, respectively. Zeng et al. [34] employed a multi-population genetic algorithm to optimize a CCHP system coupled with a ground source heat pump (GSHP) with the critical value of gas engine operation, the heating/cooling to total heating/cooling load ratio provided by the GSHP system, and the rated heat capacity of the gas engine as free variables. The results of the case study suggested that the comprehensive performance, ATCSR, CDERR, and PESR of the hybrid system were 25.42%, 15.13%, 26.10%, and 35.02%, respectively. Hou et al. [35] optimized the capacity of the main equipment in a solar-assisted CCHP system containing a heat storage tank, an electric chiller, solar evacuated tube collectors (ETC), a photovoltaic system, a heat recovery system, and a solid oxide fuel cell (SOFC) as a power generation unit using a particle swarm (PSO), aiming verify the feasibility of the proposed system architecture. However, the determination of weights in the a priori method is subjective, because the decision-maker has influences on it [36]. To explore the variation of system performance of CCHP systems under multiple parameters, researchers can use posterior multi-objective optimization algorithms [37]. Tan et al. [38] used a combination of coevolutionary theory, beetle-tentacle search algorithm, and non-dominated sorting genetic algorithm to optimize the proposed multi-objective model of the CCHP system. The simulation results indicated that the proposed hybrid algorithm has advantages in terms of global search performance and fast convergence performance. Ehyaei et al. [39] performed a multi-objective optimization of a model containing two objective functions of energy efficiency, power, and cooling cost using the multi-objective particle swarm optimization algorithm. The optimization results proved the best energy efficiency as well as power and cooling costs of 6.8% and $0.0033/kWh, respectively. Yao et al. [40] investigated the design trade-off between economic objectives and thermodynamics of a novel CCHP system based on compressed air energy storage using the multi-objective evolutionary algorithm. The optimization results revealed the best trade-off solution has a total product unit cost of 20.54 cents/kWh and total energy efficiency of 53.04%. However, as the complexity of the CCHP system increases, the most significant drawback of these algorithms is that they do not produce Pareto fronts with a high-quality uniform distribution, as they may cluster randomly [41].

Moreover, it is necessary to select a non-dominated solution in the Pareto optimal solution set as the best compromise CCHP configuration solution after multi-objective optimization, because there may exist some conflicts between different objective functions. Boyaghchi et al. [42] employed the linear programming technique for multidimensional analysis of preference (LINMAP) method and the technique of ordinal preference for similarity of ideal solutions (TOPSIS) procedure, thus determining the final optimal performance of the system from the optimal set of solutions obtained from the multi-objective optimization configuration of the CCHP system. The optimization results showed that the maximum energy efficiency and product cost improvements within 23.67% and 33.49% could be obtained by the TOPSIS procedure and the LINMAP method, respectively. Cao et al. [43] aimed to obtain the optimal compromise solution from the multi-objective optimal configuration solution set of a novel multi-generation energy system using Shannon's entropy, TOPSIS, and LINMAP conventional decision methods, respectively. Among many Multi-Criteria Decision Making (MCDM) methods developed for solving realistic decision problems, the good performance of the TOPSIS allows it to work satisfactorily in different application domains [44].

In summary, the above studies demonstrate the feasibility and effectiveness of coupling photovoltaic and solar thermal technologies with CCHP systems. However, the researches on CCHP systems coupling photovoltaic and solar thermal technologies are not comprehensive. Most studies only consider design optimization, thus ignoring the effects of operational strategies on the performance of hybrid CCHP. However, with the introduction of photovoltaic and solar thermal technologies, the constraints and variables in the hybrid system are further increased, and the general multi-objective optimization algorithm is prone to fall into local optimality in the optimization process, thereby failing to provide a Pareto front with the high-quality distribution. In addition, the coupling between equipment configuration and operation strategy is further deepened, so it is necessary to select optimization algorithms with good performance to optimize the hybrid CCHP system, as well as to develop a more appropriate operation strategy to manage the equipment in the hybrid system. Accordingly, the contribution of this study is presented as follows:

(1) Considering the economic, energy, and environmental performance of hybrid CCHP system which contains batteries, thermal energy storage tanks, gas boilers, solar heaters, photovoltaic panels, micro gas turbines, and a power grid, a multi-objective optimization model is established.

(2) To avoid the influence of local optima and objectively solve the multi-iterative energy dispatching problem, a multi-objective arithmetic optimization algorithm is proposed by introducing mutation operations, non-dominated sorting, and external archive mechanisms into the arithmetic optimization algorithm.

(3) Based on FTL and FEL operating strategies, a new operating strategy is proposed to improve the performance of the hybrid system. The proposed multi-objective algorithm optimization algorithm is used to optimize the configuration of the hybrid system under different strategies, and the optimal compromise solution is selected by the TOPSIS method.

The remainder of this paper is organized as follows: Section 3 describes the structure of the constructed hybrid CCHP system and the model of the main equipment. Section 4 shows the optimization model, the operation strategies, and the optimization algorithm. Section 5 discusses the optimization results and analyzes the system performance under different strategies. Section 6 presents the findings, contributions, and future research.

3. System description

Considering to meet the multiple demands of users, this study develops a hybrid solar combined cooling, heating, and power system, the specific structure of the system is shown in Figure 1. When the system works according to a strategy, microturbine (MT) first starts to provide heat as well as electricity to the users, and when the light intensity reaches a certain standard, Solar thermal (ST) collectors and Photovoltaic (PV) systems start to deliver heat and electricity to the users respectively, Gas boiler (GB) starts to work when the system does not produce enough heat, the battery can absorb electricity when the system has electrical energy redundancy and release electricity when the system's power generation is insufficient, Thermal energy storage (TES) tank can absorb thermal energy when the system has thermal energy redundancy and releases the stored thermal energy when the system does not produce enough heat. The grid assumes the role of the auxiliary power supply when the system's power generation is not enough to bear the demand of users.

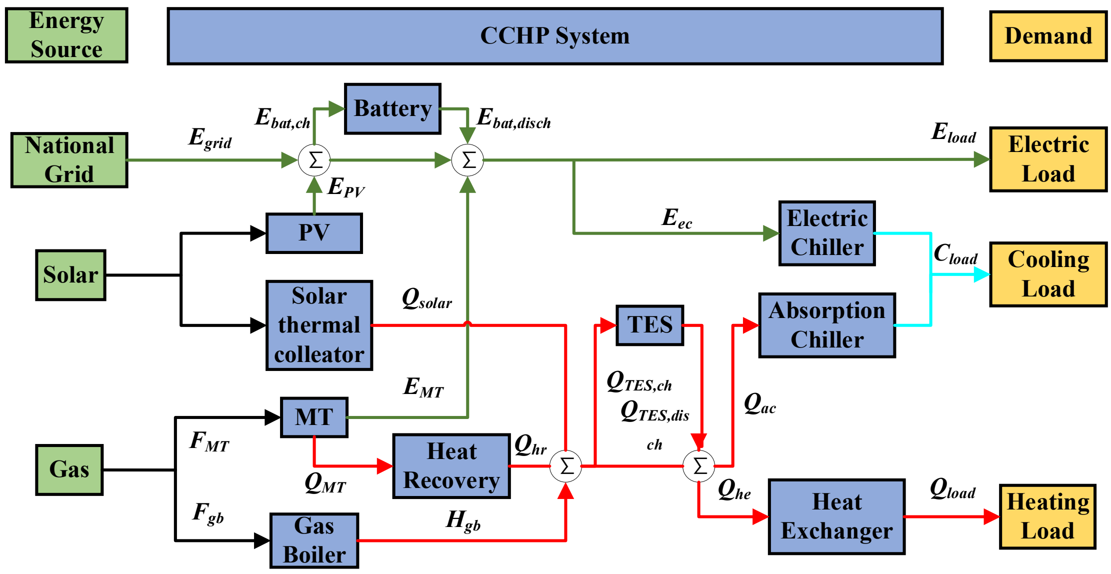

Fig 1. Structure of CCHP system.

3.1. Solar thermal collectors

The thermal energy generated by ST collectors is estimated as follows [45]:

$$Q_{st} = A_{ST} I \eta_{st} = A_{ST} I[b_0 - b_1 T^* - b_2 I(T^*)^2] \tag{1}$$

$$T^* = ((T_{out} + T_{in}) / 2 - T_a) / I \tag{2}$$

where b_0 represents the optical efficiency, b_2 and b_1 represent the correction factor. The area of the solar collector is represented by A_{ST}; I, T_{out}, T_{in}, and T_a represent the light intensity, *ST* external temperature, *ST* internal temperature, and air temperature, respectively.

3.2. Photovoltaic systems

The electricity generated by the PV systems is estimated as follows [46]:

$$E_{PV} = C_{PV} \cdot I_{PV} / I_{STC} \cdot \left[1 + \beta \cdot \left(T_{PV} - T_{STC}\right)\right] \tag{3}$$

where T_{PV} represents the PV panel surface temperature, I_{PV} represents light intensity, E_{PV} represents the electricity generated by PV; T_{STC}, I_{STC} represent the panel surface temperature and light intensity under laboratory conditions, respectively; *β* represents the temperature coefficient.

3.3. Microturbine and Waste Heat Recovery Unit

While microturbine (MT) provides electricity to customers, the waste heat generated is recovered by a waste heat recovery (HR) device to provide heat for users. The electrical energy generated by MT and heat energy recovered by HR is estimated as follows [47]:

$$E_{MT} = Fuel_{MT} \cdot \eta_{MT} \tag{4}$$

$$Q_{HR} = Fuel_{MT} \eta_r \left(1 - \eta_{MT}\right) \tag{5}$$

where η_{MT}, E_{MT}, $Fuel_{MT}$ represent the efficiency of MT power generation, the electrical energy generated by MT, and consumption of gas by MT, respectively; η_r, Q_{HR} represent the efficiency of waste heat recovery, the amount of waste heat recovery, respectively.

3.4. Thermal energy storage tank

TES reduces the thermal energy waste and replenishes the thermal energy shortage of the system by absorbing and releasing thermal energy. When the heat production of the system is greater than the heat demand of the user, TES starts to work, and this process is the heat absorption process of TES; when the heat production of the system is not enough to bear the demand of the user, TES carries out the heat release work. The heat absorption and exothermic processes of TES are calculated by the following equation [46].

$$\begin{cases} Q_{TES}^{t} = Q_{TES}^{t-1} \cdot (1 - \gamma_{TES}) + Q_{TES,ch}^{t} \cdot \eta_{TES,ch} \cdot t \\ Q_{TES}^{t} = Q_{TES}^{t-1} \cdot (1 - \gamma_{TES}) - Q_{TES,disch}^{t} / \eta_{TES,disch} \cdot t \end{cases} \tag{6}$$

where Q_{TES}^{t-1} and Q_{TES}^{t} denote the heat stored in the thermal storage device at moments *t*-1 and *t*, respectively; γ_{TES} denote the heat loss rate, $\eta_{TES,ch}$ and $\eta_{TES,disch}$ are the transportation efficiency in the process of heat charging and discharging t, respectively. $Q^{t}_{TES,disch}$ and $Q^{t}_{TES,ch}$ denote the heat released and absorbed by the TES at moment t, respectively.

3.5. Gas boiler

The GB starts to provide heat for users when all the heating equipment cannot meet the heat demand of the users, and the heat energy generated is calculated as follows [47]:

$$Q_{GB} = Fuel_{GB} \cdot \eta_{GB} \tag{7}$$

where η_{GB}, $Fuel_{GB}$, and Q_{GB} represent the heat generation efficiency, the gas consumption, and the heat production, respectively.

3.6. Absorption chiller and electric chiller

Absorption chillers use the heat emitted by the system to cover the cooling needs of the user. Electric chillers can start refrigeration work when absorption chillers cannot meet the needs of the user. The equations for calculating the refrigeration capacity of an absorption chiller and electric chiller are as follows [46,47]:

$$Q_{ac} = H_{ac} \cdot \mu_{ac} \tag{8}$$

$$Q_{ec} = E_{ec} \cdot \mu_{ec} \tag{9}$$

where Q_{ac} and Q_{ec} are the refrigeration capacity of the absorption chiller and the electric chiller, respectively, Hac represents the heat consumption when absorption chiller works, E_{ec} represents the electricity consumption when electric chiller works, μ_{ac}, and μ_{ec} are the refrigeration coefficients of absorption chiller machine and electric chiller machine, respectively.

3.7. Battery

The introduction of the battery is an important method to reduce the waste of energy in the system. When the system power generation exceeds the user's demand, the excess power is absorbed by the battery. The power stored in the battery will be released when the system power generation is insufficient. The discharging process and the charging process of the battery are calculated by the following equations [46].

$$\begin{cases} E_{bat}^{t} = E_{bat}^{t-1} \cdot (1-\lambda_{bat}) + E_{bat,ch}^{t} \cdot \eta_{bat,ch} \cdot t \\ E_{bat}^{t} = E_{bat}^{t-1} \cdot (1-\lambda_{bat}) - E_{bat,disch}^{t} / \eta_{bat,disch} \cdot t \end{cases} \tag{23}$$

where E_{bat}^{t-1} and E_{bat}^{t} are the amount of power stored in the battery at moment *t*-1 and moment *t*, respectively. $E_{bat,disch}^{t}$ and $E_{bat,ch}^{t}$ are the discharging and charging of the battery at moment *t*, respectively; λ_{bat} denote the electric loss rate, $\eta_{bat,ch}$ and $\eta_{bat,disch}$ are the transportation efficiency in the process of charging and discharging, respectively.

3.8. Constraints

The electrical energy balance is expressed as follows:

$$\begin{cases} if\ E_{PV}^{t} + E_{MT}^{t} \geq E_{load}^{t} + E_{ec}^{t} + E_{bat,ch}^{t} \\ E_{waste}^{t} = E_{PV}^{t} + E_{MT}^{t} - (E_{load}^{t} + E_{ec}^{t} + E_{bat,ch}^{t}) \\ if\ E_{PV}^{t} + E_{MT}^{t} < E_{load}^{t} + E_{ec}^{t} + E_{bat,ch}^{t} \\ E_{grid,in}^{t} = (E_{load}^{t} + E_{ec}^{t} + E_{bat,ch}^{t}) - E_{PV}^{t} - E_{MT}^{t} \end{cases} \tag{11}$$

where E_{load}^{t} represents the users' electrical energy demand at time *t*; E_{waste}^{t} represents the system power waste at time *t*; $E_{grid,in}^{t}$ represents the power purchased from the grid at time *t*; and E_{ec}^{t} represents the electric chiller power consumption at time *t*.

The heat balance of the system is shown as follows:

$$Q_{st}^t + Q_{hr}^t + Q_{tst,disch}^t + Q_{gb}^t + Q_{vacancy}^t = Q_{load}^t + Q_{ac}^t + Q_{tst,ch}^t + Q_{waste}^t \tag{12}$$

in which $Q_{vacancy}^t$ represents the thermal energy vacancy of the system at moment *t*; Q_{waste}^t represents the thermal energy wasted by the system at moment *t*.

4. Problems and optimization methods

This study establishes a hybrid system optimization model including environmental, energy, and economic objective functions and adopts MOAOA to optimize the configuration of the hybrid system, the optimization model and the optimization algorithm are described in detail as follows.

4.1. Decision variables

For hybrid CCHP systems, the MT plays a decisive role in determining the capacity of the other equipment as the core component for supplying energy to the customer, the GB, as a key component of auxiliary heating, plays a key role in avoiding insufficient heat production in the system. As a renewable energy source, the introduction of photovoltaics and solar thermal collectors increases the diversity of system energy sources and reduces carbon emissions and fossil fuel consumption. However, their output is uncertain. Therefore, the optimal PV capacity and ST capacity may lead to a trade-off between installed capacity and initial investment. In addition, user's load demand, light intensity, and temperature are in a state of flux, energy storage devices also have a positive effect on the performance of the system. Therefore, to obtain the optimal installed capacity of hybrid CCHP system equipment, seven equipment capacities of the system were selected as decision variables.

$$X = \left[V_{grid}, V_{TES}, V_{bat}, V_{GB}, V_{ST}, V_{PV}, V_{MT} \right] \tag{13}$$

in which V_{grid} indicates the upper limit of power purchased from the grid by the system; V_{TES}, V_{bat}, V_{GB}, V_{ST}, V_{PV}, V_{MT} are capacities of TES, battery, GB, ST, PV, MT, respectively. The upper and lower capacity limits for each device and the charging and discharging constraints for the battery and TES are shown in Table 1.

Table 1. The upper and lower bounds of the hybrid system equipment capacity.

Device	Value	Unit
Capacity of Grid	[0, 300]	kW
Charge and discharge limit of Battery	(0, 0.4V_{bat})	kW
Charge and discharge limit of TES	(0, 0.4V_{TES})	kW
Capacity of Battery	[0, 200]	kW
Capacity of TES	[0, 300]	kW
Capacity Gas Boiler	[0, 1000]	kW
Area of ST	[0,500]	m^2
Capacity of PV	[0,300]	kW
Capacity of MT	[0,500]	kW

4.2. Objective functions

The greenhouse gas emissions, fuel consumption and economic cost objective functions of the system are established to evaluate the comprehensive performance of the system.

(1) Greenhouse gas emissions

The greenhouse gas emissions objective function is defined as follows:

$$f_1 = \sum_{t=1}^{T}\left(E_{grid,in} \cdot \beta_{CO_2,e} + (Fuel_{MT} + Fuel_{GB}) \cdot \beta_{CO_2,g}\right) \tag{14}$$

where $E_{grid,in}$ represents the electricity purchased from the grid, $Fuel_{GB}$ and $Fuel_{MT}$ represent the consumption of GB and MT fuel, respectively; $\beta_{CO_2,e}$ and $\beta_{CO_2,g}$ represent the equivalent emission factors of electricity and the grid, respectively.

(2) Fuel consumption

The fuel consumption objective function for the system is defined as follows：

$$f_2 = \sum_{t=1}^{T}(Fuel_{MT}^{t} + Fuel_{GB}^{t} + Fuel_{grid}^{t}) \tag{15}$$

where $Fuel_{MT}^{t}$, $Fuel_{GB}^{t}$ and $Fuel_{grid}^{t}$ represent the MT, GB and grid fuel consumption during system operation, respectively.

(3) Economic cost

The operating cost of the system consists of the initial investment cost, the cost of purchasing power from the grid, the fuel consumption cost, and the penalty cost. This study sets the penalty cost to maximize the use of electrical and thermal energy in the optimization process. The above four components of operating cost can be calculated as follows:

$$C_{inv} = p \cdot \sum_{i=1}^{n} V_k \cdot C_k \tag{16}$$

$$C_{grid} = \sum_{t=1}^{T} E_{grid,in}^{t} \cdot C_e \tag{17}$$

$$C_{fuel} = \sum_{t=1}^{T}\sum_{i=1}^{k} Fuel_k^{t} \cdot C_f \tag{18}$$

$$C_{waste} = \sum_{t=1}^{T}\left(\lambda_e \cdot E_{waste}^{t} + \lambda_h \cdot Q_{waste}^{t}\right) \tag{19}$$

$$f_3 = C_{inv} + C_{grid} + C_{fuel} + C_{waste} \tag{20}$$

where p denotes the investment coefficient; C_k, N_k represent the unit investment cost and installed capacity of the kth device, respectively; $E^t_{grid,in}$ is the amount of electricity purchased by the system from the grid at time t; $Fuel^t_k$ denotes the amount of gas consumed by the kth equipment during the operation time; C_f and C_e represent the price of fuel and electricity, respectively; E^t_{waste} and Q^t_{waste} are the amount of electricity and heat energy wasted by the system, respectively; λ_e, λ_q are the penalty coefficients for electricity and heat energy wastage, respectively; T represents the total operation time.

4.3. Operation strategy

To reduce energy redundancy and waste in the system, this study proposes a strategy for following the state of battery energy storage based on the traditional FTL and FEL strategies.

(1) FEL strategy

When the system is running under the FEL strategy, the MT starts to provide electricity for the customers first. When the light intensity reaches a certain standard, the photovoltaic system starts to generate electricity to meet the users' demand, and when the MT and photovoltaic power generation are not enough to meet the users' demand, a part of electricity will be purchased from the grid to meet the needs of users. In terms of system heat supply, the heat recovered in the MT power generation process provides heat for the users, and the ST starts to provide heat for the users when the light intensity reaches a certain standard. The GB plays its role of auxiliary heat supply when the above two parts of heat cannot meet the needs of the users, however, the excess heat will be stored in when the recovered heat in the MT power generation process and the heat generated by the ST exceeds the heat required by the users, and when the heat stored in the TES exceeds its capacity limit, there is a waste of heat energy.

(2) FTL strategy

When the system operates under the FTL strategy, the MT first starts to work to provide thermal energy to the customers. When the light intensity reaches a certain standard, ST starts to generate thermal energy to meet the thermal energy demand of users. When the thermal energy recovered during MT generation and the thermal energy generated by ST is not enough to meet the thermal energy demand of users, GB starts to play its role of auxiliary heat supply. For the system power supply, the power generated by MT will first provide electricity for users, and when the light intensity reaches a certain standard, the PV system will start to work to provide electricity for users, and when the above two parts of electricity cannot meet the needs of users, electricity will be purchased from the grid to meet the electricity needs of users. When the power generated by the MT and PV system exceeds the power required by users, the excess power will be stored in the battery, and when the power stored in the battery exceeds its capacity limit, there will be a waste of power.

(3) FB strategy

This study proposes a strategy for following the state of the battery (FB). The energy storage status of the battery will be detected during system operation, and when the battery dischargeable criterion is reached, the system will execute the FEL strategy. On the contrary, when the stored energy in the battery is less than the dischargeable standard, the system will execute the FTL strategy, and the excess power will be stored by the battery during operation, and when the battery dischargeable standard is reached, the system will execute the FEL strategy again. The FB strategy can switch the strategy according to the stored energy state of the battery.

4.3. Optimization method

Arithmetic optimization algorithm (AOA), as a novel heuristic algorithm, can optimize problems containing multiple constraints, and the output is highly competitive. To obtain uniformly distributed Pareto solutions and reduce clustering of solutions, this study introduces non-dominated sorting, external archive mechanism and mutation operations to the original AOA to obtain MOAOA.

4.3.1. Arithmetic optimization algorithm

AOA, inspired by the behaviors of the distributions of arithmetic operators commonly used in math [48]. The exploitation phase and exploration phase are the two main phases of its search process. In the AOA search process, a math optimization accelerator is used as a coefficient to select the exploration or utilization, whose value is defined as:

$$MOA(iter) = MIN + iter \times (MAX - MIN) / Max\_iter \tag{21}$$

where *MAX* and *MIN* represent the maximum and minimum values of the optimizer, respectively.

(1) Exploration phase

The AOA exploration operator performs random exploration on multiple regions of the search space, and its search mechanism is based on the division search mechanism and multiplication search mechanism to find better candidate solutions. The mathematical expression of the search mechanism is defined as follows:

$$w_j = ((ub_j - lb_j) \times \mu + lb_j) \tag{22}$$

$$x_{i,j}(iter+1)=\begin{cases} best_j \div (MOP+\in)\times w_j, & r_2<0.5 \\ best_j \times MOP \times w_j, & otherwise \end{cases} \tag{23}$$

$$MOP(iter)=1-1/Max\_iter^{1/Delta} \tag{24}$$

where μ is an adjustable variable used to regulate the search process, *iter* is the current number of iterations, $\in$ is a small integer, $best_j$ denotes the *j*th coordinate of the optimum individual of the current iteration, $x_{i,j}(iter)$ is the *j*th coordinate of the *i*th individual under the current number of iterations, lb_j and ub_j denote the lower and upper bounds of the *j*th coordinate, respectively. The coefficient of the math optimization accelerator is represented by *MOP*, *Delta* is a sensitive parameter that represents the development precision during the process of iteration.

(2) Exploitation phase

In the algorithm exploitation phase, compared to other operators, the mathematical operators of addition and subtraction have low dispersion but high density and use in the exploitation phase to infer the candidate that is closer to the optimal value through multiple iterations. The mathematical model is defined as follows:

$$x_{i,j}(iter+1)=\begin{cases} best_j - (MOP+\in)\times w_j, & r_3<0.5 \\ best_j + MOP \times w_j, & otherwise \end{cases} \tag{25}$$

4.3.2. Multi-objective arithmetic optimization algorithm

In this study, MOAOA is obtained by introducing mutation operation, external archive, and non-dominated sorting mechanism in AOA.

(1) polynomial mutation

The variation operator performs random variation operations on individuals according to certain variation probabilities, and in this study, the polynomial mutation is utilized in the elite solution set to increase the diversity of the population [49].

$$p_k' = p_k + \delta(ub_k - lb_k) \tag{26}$$

$$\begin{cases} [2u + (1-2u)(1-\delta_1)^{\eta_m+1}]^{1/\eta_m+1} & if\ \ u \le 0.5 \\ 1-[2(1-u)+2(u-0.5)(1-\delta_2)^{\eta_m+1}]^{1/\eta_m+1} & if\ \ u > 0.5 \end{cases} \tag{27}$$

$$\delta_1 = (p_k - lb_k)/(ub_k - lb_k) \tag{28}$$

$$\delta_2 = (ub_k - p_k)/(ub_k - lb_k) \tag{29}$$

where p_k denotes a parent individual, u represents a number between 0 and 1, and η_m is the distribution index.

(2) Cauchy mutation

The inclusion of the Cauchy mutation not only maintains population diversity but also allows the algorithm to avoid falling into local optima when solving a complex optimization problem [50].

$$\begin{cases} P_i = P_i \times (1 + 0.3 \times Cauchy(0,1)) \\ Cauchy(0,1) = \tan((rand - 0.5) \times \pi) \end{cases} \tag{30}$$

where P_i is the current position, *rand* is a random value uniformly distributed in [0,1], $Cauchy(0,1)$ is a standard Cauchy-distributed random value.

(3) Crowding distance

The crowding distance is utilized to characterize the distribution of non-dominated solutions. In the solution set obtained by the algorithm, each non-dominated solution has a crowding distance, which is utilized to represent the sum of the distances of the nearest non-dominated solutions in each objective function dimension. While in the boundary solutions in the Pareto front, the crowding distance is set to inf, and the crowding distance of other solutions is defined as:

$$P(i)_{distance} = \sum_{m=1}^{D} (P(i+1).m - P(i-1).m) / f_m^{\max} - f_m^{\min} \tag{31}$$

where D represents the dimensionality of the objective function, $P(i\text{-}1).m$ denotes the mth dimensional objective function value that is second only to the ith solution after sorting the mth objective function value in the non-dominated solution set, $f_m^{\min}$ and $f_m^{\max}$ represent the minimal and maximal of the mth objective function value, respectively.

(4) Non-dominated sorting

First, all non-dominated individuals in the population are identified to obtain the first non-dominated optimal layer; then, the individuals in the first non-dominated layer are ignored and the other individuals in the population are stratified according to the dominant-non-dominated relationship to obtain the second non-dominated optimal layer, and the above operation is continued for the remaining individuals until all individuals in the population are stratified.

The above describes the process of introducing a non-dominated sorting mechanism and an external archive mechanism to form MOAOA in AOA. The flow chart of MOAOA is displayed in Figure 2.

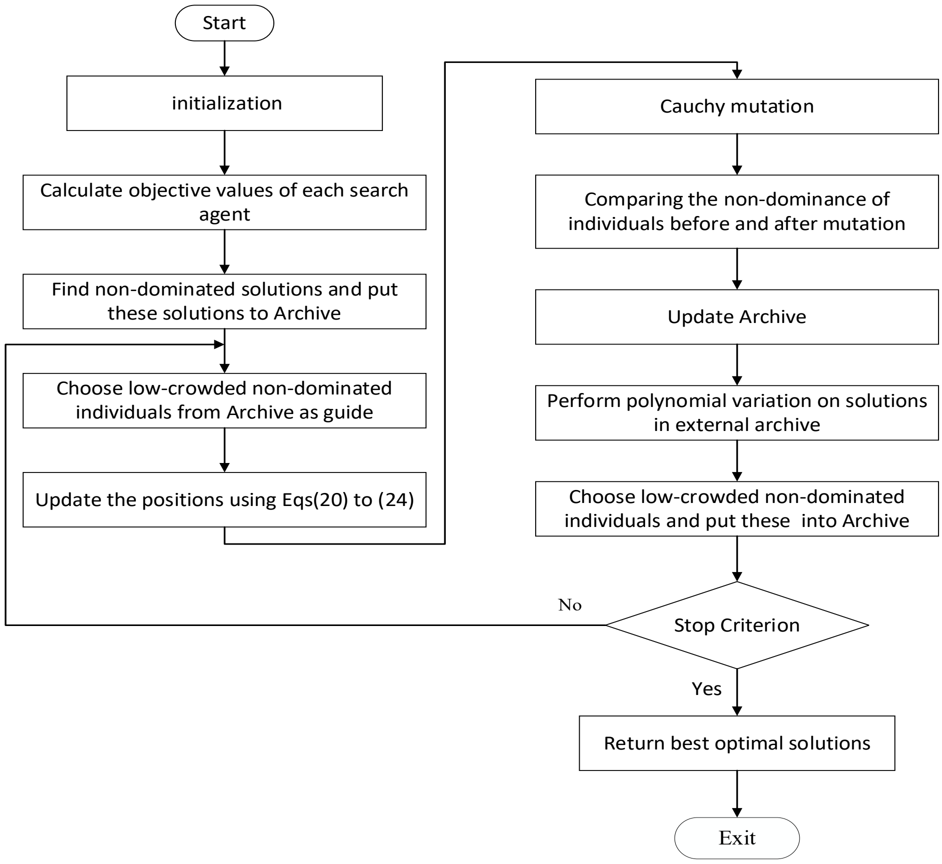

Fig 2. Flowchart of the proposed MOAOA algorithm.

(5) TOPSIS Decision-making

When solving a problem using a multi-objective optimization algorithm, the optimal compromise solution is not directly available, so it is necessary to use certain methods to process the optimal solution set to select the optimal compromise solution. In this study, the TOPSIS method is used in the decision phase to select from the optimal set of solutions.

(1) Decision Matrix Normalization

$$\delta_{i,j} = \gamma_{i,j} \Big/ \sqrt{\sum_{i=1}^{M} \gamma_{i,j}^{2}} \quad i = 1, 2 \cdots M-1, M; \quad j = 1, 2, 3 \tag{32}$$

$$\gamma_{i,j} = \max_{i}\left(b_{i,j}\right) - b_{i,j} \tag{33}$$

in which $\delta_{i,j}$ represents the normalized elements; M represents the number of optimal solutions; $b_{i,j}$ represents the elements in decision-making matrix; $\gamma_{i,j}$ represents the formalized elements.

(2) Optimal and inferior solution calculation

$$\begin{cases} \gamma_j^+ = \max\limits_i(\delta_{i,j}) \quad j = 1,2,3 \\ \gamma_j^- = \min\limits_i(\delta_{i,j}) \quad j = 1,2,3 \end{cases} \tag{34}$$

in which γ_j^+ and γ_j^- represent the optimal solution and the inferior solution, respectively.

(3) Calculation of distance

$$\begin{cases} Dis_i^+ = \sqrt{\sum_{j=1}^{3}\left(\gamma_{i,j} - \gamma^+\right)^2} \\ Dis_i^- = \sqrt{\sum_{j=1}^{3}\left(\gamma_{i,j} - \gamma^-\right)^2} \end{cases} \tag{35}$$

in which Dis_i^+ and Dis_i^- are the distances of the *i*th optimum solution to the optimal and inferior solution, respectively.

(4) Comprehensive distance calculation

$$W_i = Dis_i^- / (Dis_i^+ + Dis_i^-) \tag{36}$$

in which W_i represents the comprehensive distance, and the larger W_i means the higher score of the *i*th compromise solution.

4.4. Testing of algorithm performance

The series of ZDT (ZDT1-ZDT4, ZDT6) [51] test functions are adopted for the algorithm performance comparison experiments in this study. The algorithms for convergence performance comparison with MOAOA in this study consist of multi-objective evolutionary based on decomposition (MOEA/D) and multi-objective particle swarm optimization (MOPSO).

To ensure the fairness of the comparison experiment, the proposed algorithm and the comparison algorithms are run 30 times independently on each test function. The population size is 100 and the maximum number of iterations is 100. Inverted Generation Distance (IGD)

[52] is used to evaluate the distribution performance and convergence performance of an algorithm. IGD evaluates the overall performance of an algorithm by computing the minimum sum of distances between each solution on the real Pareto front surface and the set of solutions obtained by the algorithm. The smaller the value, the better the convergence and distribution performance of the algorithm. Spacing metric (SP) [53] is a measure of the uniformity of the solution set distribution obtained by the algorithm by calculating the standard deviation of the minimum distance of each solution to the other solutions. The smaller the Spacing value, the more uniform the solution set is.

(1) Inverted Generation Distance

$$\mathrm{IGD}=\frac{\sum_{i=1}^{n} d_i}{n} \tag{37}$$

where the shortest Euclidean distance among all points on the true frontier and the vectors in the target space is represented by a d_i.

(2) spacing metric

$$\mathrm{SP}=\sqrt{\frac{1}{n-1}\sum_{1}^{n}(\bar{d}-d_i)^2} \tag{38}$$

where $\bar{d}$ represents the average of all shortest Euclidean distances, d_i denotes the minimum Euclidean distance from the ith solution in the solution set to the other solutions, and n is the number of solutions.

The performance metrics of MOAOA and the comparison algorithm on the ZDT test functions are shown in Table 2, Table 3. The results show that the proposed multi-objective arithmetic optimization algorithm can provide the best results on all statistical metrics of ZDT, and IGD is the performance measure that shows the accuracy and convergence of the algorithm. The MOAOA algorithm can provide superior convergence on ZDT. Similarly, the spacing metric is a performance measure of the uniformity of the distribution of the solutions obtained by the algorithm. Therefore, it can also be shown that MOAOA is able to provide solutions with more uniform distribution.

Table 2. The SP statistics on ZDT1-ZDT4 and ZDT6.

	MOAOA				MOEA/D				MOPSO			
SP	Average	Std	Worst	Best	Average	Std	Worst	Best	Average	Std	Worst	Best
ZDT1	5.85E-03	3.51E-04	6.39E-03	5.50E-03	6.23E-02	4.51E-02	1.09E-01	9.47E-03	1.21E-02	4.75E-02	1.62E-02	8.96E-03
ZDT2	5.32E-03	3.95E-04	5.98E-03	4.92E-03	2.46E-02	1.49E-02	4.65E-02	1.23E-02	4.67E-02	3.23E-03	7.35E-02	1.98E-02
ZDT3	6.28E-03	8.63E-04	7.31E-03	5.60E-03	1.21E-01	1.75E-01	4.32E-01	2.34E-02	3.35E-02	4.25E-02	4.65E-02	1.91E-02
ZDT4	5.87E-03	5.49E-04	6.36E-03	5.18E-03	6.50E-01	3.73E-01	1.08E+00	1.90E-01	2.64E+00	1.13E-02	5.15E+00	1.23E-01
ZDT6	5.05E-03	4.34E-04	5.73E-03	4.60E-03	5.99E-02	4.75E-02	1.34E-01	2.28E-02	8.72E-02	3.33E-01	2.22E-01	1.86E-02

Table 3. The IGD statistics on ZDT1-ZDT4 and ZDT6.

	MOAOA				MOEA/D				MOPSO			
IGD	Average	Std.	Worst	Best	Average	Std	Worst	Best	Average	Std	Worst	Best
ZDT1	4.63E-03	1.95E-04	4.93E-03	4.43E-03	6.23E-02	7.39E-02	1.25E-01	2.97E-01	1.21E-02	7.52E-03	3.33E-02	1.48E-02
ZDT2	4.54E-03	2.58E-04	4.96E-03	4.32E-03	1.05E+00	6.33E-01	1.61E+00	8.45E-03	2.98E-01	2.90E-01	7.72E-01	2.46E-02
ZDT3	6.12E-03	1.24E-03	7.11E-03	4.68E-03	7.68E-02	1.18E-01	2.86E-01	8.72E-03	6.05E-02	1.72E-02	8.76E-02	4.13E-02
ZDT4	4.80E-03	2.70E-04	5.22E-03	4.47E-03	3.71E+00	2.33E+00	6.45E+00	7.77E-01	4.75E+01	2.43E+01	7.45E+01	1.94E+01
ZDT6	3.33E-03	4.37E-04	3.82E-03	2.69E-03	5.69E-02	2.02E-02	8.47E-02	3.55E-02	5.16E-01	1.14E+00	2.55E+00	3.89E-03

Figure 3 provides the Pareto optimal fronts obtained by the three algorithms on the test functions ZDT1-ZDT4 and ZDT6. The convergence status of the three algorithms on the ZDT1 test function is displayed in Figure 3(a). The solution set obtained by the proposed MOAOA can effectively and uniformly converge to the true Pareto front, however, MOEA/D can only converge to the first half of the true Pareto front, while MOPSO cannot efficiently converge to the true Pareto front, which is also confirmed by the local enlargement shown in Figure 3(a). The convergence of the three algorithms on the ZDT2 test function is shown in Figure 3(b). The solution set of MOAOA converges uniformly to the true Pareto front. However, the solution set of MOPSO does not converge to the true Pareto front, and the solution set of MOEA/D converges well at the front end of the true Pareto front, but does not fully converge to the true Pareto front after the second half. The results are also confirmed by the local enlargement shown in Figure 3(b). The convergence of the three algorithms on the ZDT3 test function is shown in Figure 3(c), and the solution set of the proposed algorithm converges uniformly to the true Pareto front, while the solution set of MOEA/D falls into the local optimum, and the solution set of MOPSO fails to converge to the true Pareto front. The convergence states of the three algorithms for the ZDT4 test function are shown in Figure 3(d). The solution set of the proposed algorithm converges to the true Pareto front homogeneously, while the solution sets of both MOEA/D and MOPSO fail to converge to the true Pareto front. The convergence status of the three algorithms with respect to the ZDT6 test function is shown in Figure 3(e), the solution set of the proposed algorithm converges homogeneously to the true Pareto front, however, the solution set of MOEA/D does not converge to the true Pareto front, while a large portion of the solution set of MOPSO converges to the true Pareto front, but their distribution is uneven.

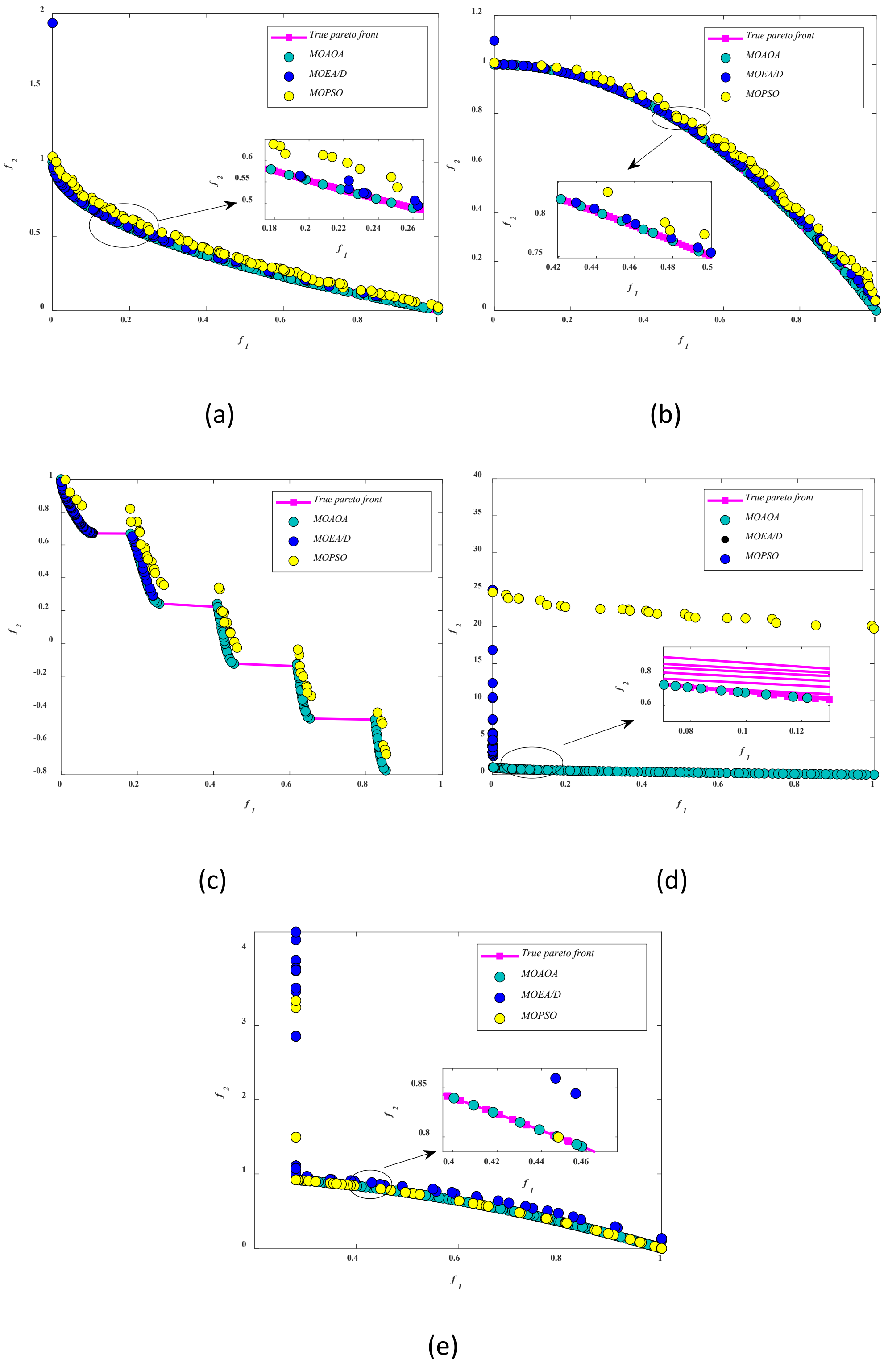

Fig 3. Pareto fronts of different algorithms on test problems ZDT1-ZDT4 and ZDT6

5. Results and discussions

Large hotels have a steady demand for electricity, heating, and cooling throughout the year. Therefore, in this study, the load data of a large hotel, one of the 16 commercial reference buildings provided by the U.S. Department of Energy (DOE) [54], is used as a case study to simulate and analyze the established solar combined cooling, heating and power system using the proposed optimization algorithm.

In this study, the operating conditions of typical days are chosen in order to illustrate more clearly the output of each equipment of the hybrid system under the three strategies. Typical daily load curves for a large hotel are depicted in Figure 4 [55]. The reference hotel has a steady electrical load throughout the year, and the heating load demand increases as the weather gets colder and the cooling load demand decreases as the weather gets warmer. In addition, since the load curves for spring and fall are similar, spring and fall are considered as the transition season, separate operation analyses for spring and fall are no longer conducted. To ensure the universality of the hybrid system under the proposed strategy, a day with relatively low heat load demand and high cooling load demand in summer was chosen as a typical summer day, and a day with high heat load demand and low cooling load demand in winter was chosen as a typical winter day.

The technical parameters of the equipment are shown in Table 4.

Table 4. Equipment technical parameters of hybrid CCHP system.

Equipment	Value	Symbol	Parameter
Thermal energy storage tank [46]	0.8	$\eta_{TES,disch}$, $\eta_{TES,ch}$	Discharge/charge efficiency
	0.04	$\eta_{TES,loss}$	Self-exothermic rate
Battery [46]	0.95	$\eta_{bat,disch}$, $\eta_{bat,ch}$	Discharge/discharge efficiency
	0.04	$\eta_{bat,loss}$	Self-discharge rate

Gas boiler [47]	0.8	η_{GB}	Efficiency
Heat exchanger [47]	0.8	η_{he}	Efficiency
Heat recovery [46]	0.8	η_{HR}	Efficiency
MT [46]	0.3	η_{MT}	Efficiency
Electric chiller [46]	3	PC_{ec}	Performance coefficient
Absorption chiller [47]	0.7	PC_{ac}	Performance coefficient

The unit investment costs of the equipment in the hybrid system are shown in Table 5.

Table 5. Unit price of equipment of the hybrid CCHP system.

Equipment	Price	unit
Thermal energy storage tank [46]	33	$/Kw
Battery [46]	33	$/Kw
Gas boiler [47]	42.8	$/Kw
Heat exchanger [47]	22	$/Kw
ST [48]	200	$\$/m^2$
MT [46]	969.7	$/Kw
PV [47]	2039	$/Kw
Electric chiller [46]	350	$/Kw
Absorption chiller [47]	225	$/Kw

The fuel prices and electricity prices are shown in Table 6.

Table 6. Gas and electricity prices [47].

	Period	Unit price($/kWh)
	23:00-7:00	0.0547
	7:00-10:00, 15:00-16:00,	0.1285
	17:00-18:00, 21:00-23:00	0.1285
Electricity	10:00-11:00, 13:00-15:00,	0.2060
	18:00-21:00	
	11:00-13:00, 16:00-17:00	0.2252
Natural gas	---	0.0366

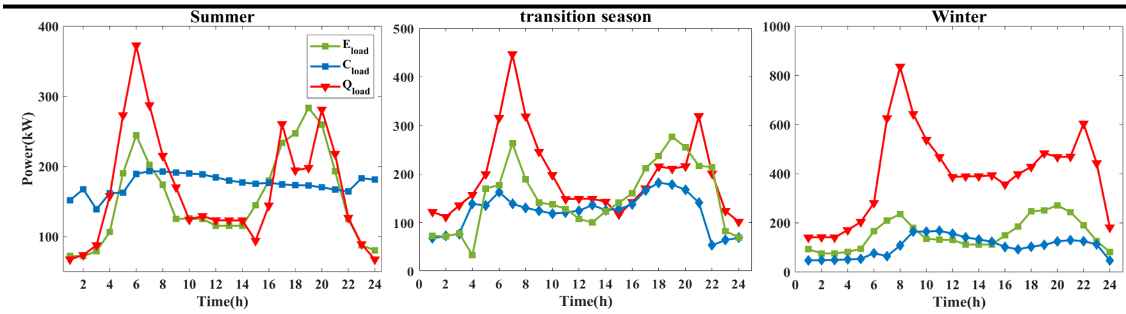

Fig 4. Hourly energy demand of typical days.

This study utilizes MOAOA to optimize the configuration of hybrid and traditional systems running under different strategies. The MOAOA parameters are set as follows: maximum number of iterations, number of populations, and maximum number of external archive stores are set to 500,100,100, respectively. The research experiments are conducted on Matlab2021a running on Intel(R) Core (TM) i5-5200U CPU 2.20Ghz, 12GB of RAM, and Windows 10 operating system.

5.1. Optimization results

The system is optimized using MOAOA, and the Pareto solution of traditional and hybrid systems operating under the three strategies is shown in Figure 5.

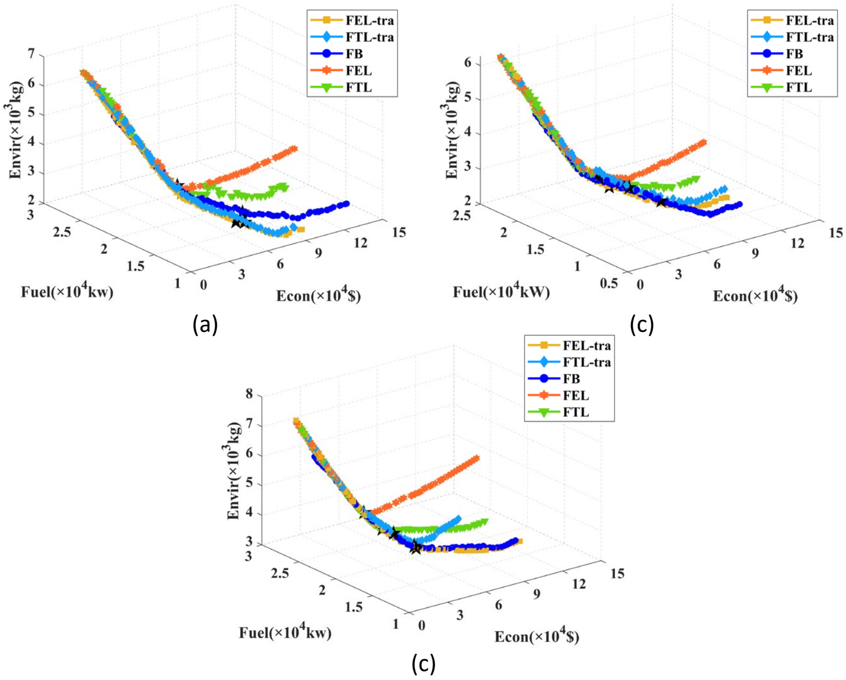

Fig 5. The Pareto scheme gained by MOAOA under various strategies.

FEL-tra represents traditional CCHP running under FEL strategy, FTL-tra represents traditional CCHP system running under FTL strategy, FB represents hybrid system running under the proposed strategy, FEL represents hybrid system running under FEL strategy, FTL represents hybrid system running under FTL strategy.

Figure 5(a) shows the spatial distribution of the Pareto solutions obtained by optimization through MOAOA on a typical summer day. Each point in Figure 5(a) represents the optimal solution obtained in the external archive concerning the three objective functions, and the optimal set of solutions obtained for the system running under the different operation strategies has a similar distribution, and it is clear that MOAOA provides multiple solutions for the optimal configuration of the CCHP system. The distribution of the Pareto solution shows that the hybrid system has a better performance concerning fuel consumption and greenhouse gas emissions. In addition, the optimal compromise determined by TOPSIS is marked with a black pentagram in Figure 5(a).

Figure 5(b) shows the spatial distribution of the Pareto solution obtained by MOAOA optimization on a typical day of the transition season. Each point in Figure 5(b) is the optimal solution obtained by MOAOA concerning the economy, fuel, and environment objective functions. Similarly, the obtained set of Pareto solutions is uniformly distributed in space. Moreover, the distributional behavior of the Pareto solution set indicates that both fuel consumption and greenhouse gas emissions of the hybrid system have smaller values.

Figure 5(c) displays the spatial distribution of the Pareto solution obtained by MOAOA optimization on a typical day of the winter season. Each point in Figure 5(c) is an optimal compromise solution obtained by MOAOA concerning the three objective functions of economy, fuel, and environment. In addition, the behavior of the spatial distribution of the optimal solution is of uniformity. The optimal solution of the hybrid system performs better in terms of fuel and environmental performance.

In summary, the spatial distribution of Pareto solutions for conventional and hybrid systems under different strategies indicates that hybrid systems have better environmental and energy performance. However, the cost of the hybrid system is higher because there is more equipment in the hybrid system. In addition, the uniformity of the obtained Pareto solutions distribution indicates the effectiveness of the developed multi-objective optimization algorithm.

5.2. Performance evaluation indicators

Five basic indicators, consisting of system energy efficiency (η_{CCHP}), boiler energy savings rate (*BESR*), carbon dioxide reduction rate (*CDERR*), primary energy savings rate (*PESR*), and cost savings rate (*CSR*), are utilized in this study to evaluate the performance of the system.

The η_{CCHP} indicator is used to evaluate the relationship between inputs and outputs, the *BESR* indicator is used to reflect the operation of boilers in the system, the *PESR* indicator is used to evaluate the primary energy use in the system, the *CDERR* indicator is used to evaluate the greenhouse gas emissions of the system, and the *CSR* indicator is used to evaluate the economic cost of the system.

The η_{CCHP} is used to represent the ratio between the output and the input of the system, it is defined as follows [56]:

$$\eta_{CCHP}=\frac{E_{load}+Q_{load}+C_{load}}{Fuel+\sum_{t=1}^{T}E_{PV}^{t}+\sum_{t=1}^{T}Q_{ST}^{t}} \tag{39}$$

where E_{load}, Q_{oad}, C_{load}, *Fuel*, E_{PV}^{t} and Q_{ST}^{t} denote the customer's electrical energy demand, thermal energy demand, cooling demand, fuel consumption, electricity generated by PV, and heat generated by ST, respectively.

The *BESR* is used to evaluate the fuel consumption of the boiler in system and is calculated as follows:

$$BESR=\frac{BEC_{SP}-BEC_{CCHP}}{BEC_{SP}} \tag{40}$$

where the fuel consumption of GB in system is represented by the *BEC*.

PESR is used to evaluate the primary energy consumption of the system, *PESR* indicator of the system is calculated as follows：

$$PESR=\frac{Fuel_{SP}-Fuel_{CCHP}}{Fuel_{SP}} \tag{41}$$

where the fuel consumption of system is represented by the *PESR*.

CDERR is used to evaluate the greenhouse gas emissions from the system, *CDERR* indicator is estimated as follows：

$$CDERR = \frac{CDE_{SP} - CDE_{CCHP}}{CDE_{SP}} \tag{42}$$

where the carbon dioxide emissions of system are represented by *CDE*.

CSR is used to evaluate the cost of the system. *CSR* indicator is estimated as follows:

$$CSR = \frac{Cost_{SP} - Cost_{CCHP}}{Cost_{SP}} \tag{43}$$

where the economic cost of the system is represented by *CSR*.

A set of feasible solutions are obtained by MOAOA. The optimum solution is acquired by the TOPSIS approach from the set of solutions. The performance metrics of the optimal compromise solution are shown in Figure6.

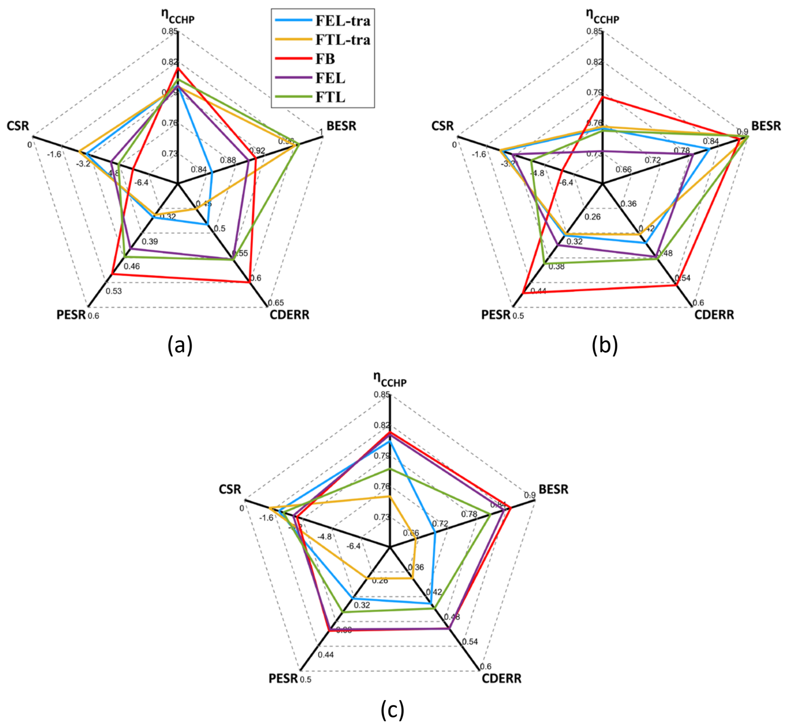

Fig 6. Performance metrics under different strategies.

FEL-tra represents traditional CCHP running under FEL strategy, FTL-tra represents traditional CCHP system running under FTL strategy, FB represents hybrid system running under the proposed strategy, FEL represents hybrid system running under FEL strategy, FTL represents hybrid system running under FTL strategy.

Figure 6(a) shows the performance metrics of the conventional and hybrid systems during a typical summer day. Figure 6(a) reveals that the *PESR*, *CDERR*, and η_{CCHP} indexes of the hybrid system are better than those of the conventional system. The *CSR* value for the solar hybrid system operating under the proposed strategy is -5.54, which is slightly worse than the *CSR* values under the FTL and FEL strategies. For *PESR*, the *PESR* value of 0.51 for FB strategy is better than the *PESR* of a hybrid CCHP system running under two other basic strategies, which indicates that the system can reduce primary energy consumption by running the proposed FB strategy. For *CDERR*, the proposed strategy has a *CDERR* value of 0.60, which is better than *CDERR* under FTL and FEL strategies, which indicates that the system can significantly achieve carbon dioxide emission reduction under the proposed FB strategy. For *BESR*, the *BESR* indicator of the proposed FB strategy is second only to that of the FTL strategy. For system efficiency, the solar hybrid CCHP system running under the proposed FB strategy eliminates waste of electrical energy and thermal waste, thus its system efficiency is the highest with a value of 0.81.

Figure 6(b) presents the operational performance metrics of the conventional and hybrid systems during a typical transition season day. The η_{CCHP}, *CDERR*, and *PESR* of the hybrid system are better than those of the traditional system, but the CSR index of the hybrid system performs worse due to the introduction of more equipment. The *CSR* value of the solar hybrid CCHP system operating under the proposed FB strategy is -5.78, which is slightly worse than the CSR values under the FTL and FEL strategies. In terms of PESR, the hybrid system running under the FB strategy has a PESR value of 0.47, which indicates that a significant reduction in primary energy consumption is achieved by the hybrid system running under the proposed FB strategy. In terms of *CDERR*, the *CDERR* value under the proposed FB strategy is 0.55, which indicates that the hybrid system operating under the proposed FB strategy can achieve significant greenhouse gas emission reductions. As for the BESR, the BESR value for the hybrid system running under the FB strategy is 0.88, which indicates that the energy consumption of the gas boiler of the hybrid system under the proposed strategy is less. In terms of system efficiency, the solar hybrid CCHP system has no energy wastage when operating under the proposed strategy, and therefore has the highest efficiency of 0.78.

Figure 6(c) presents the operational performance metrics of the traditional and hybrid systems during a typical day in winter. Figure 6(c), the hybrid system outperforms the conventional CCHP system in terms of η_{CCHP}, *CDERR*, and *PESR*. *CSR* value of solar hybrid CCHP system running proposed strategy is -2.89, which is slightly worse than the CSR values under the FTL and FEL strategies. For *BESR*, *CDERR*, and *PESR*, the values of *BESR*, *CDERR*, and *PESR* for the solar hybrid CCHP system running under the proposed strategy are 0.85, 0.50, and 0.40, respectively. The proposed strategy enables the hybrid system to have better energy and environmental performance than the hybrid system running under the FEL and FTL strategies. In addition, the hybrid system under the proposed strategy generated no energy waste, the system efficiency value of the hybrid system running under the proposed strategy is 0.81.

In summary, this study employed MOAOA for the system optimization configuration of both traditional and hybrid systems. Firstly, the hybrid system outperformed the traditional CCHP system in energy and environmental performance. Secondly, the solar hybrid CCHP system operated under the proposed strategy produced no energy waste, and the obtained evaluation indexes performed well except for the cost-saving ratio. These fully demonstrate the excellent performance of the proposed FB strategy in fuel-saving, environmental pollution reduction, and system efficiency improvement.

5.3. Analysis of operation

The optimum solution is selected from the set of solutions obtained by MOAOA using the TOPSIS method, the operation of the optimal solution is also analyzed, the results are as follows.

5.3.1. Analysis of operation in a representative summer day

The operation of the system during a typical summer day is as follows:

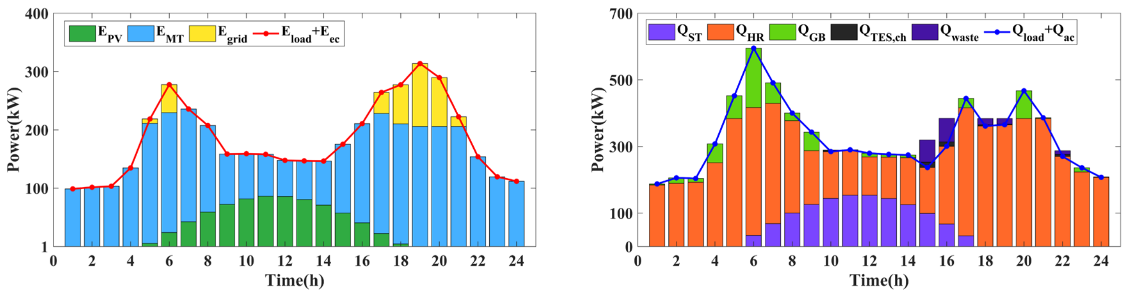

(a) (b)

Fig 7. FEL energy balance in a representative summer day.

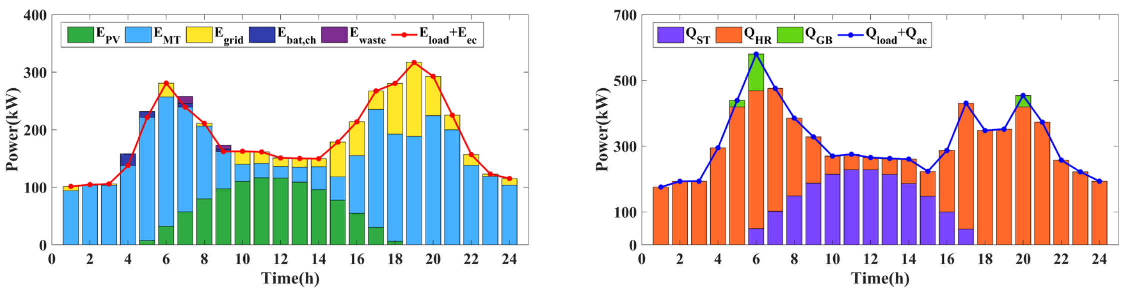

(a) (b)

Fig 8. FTL energy balance in a representative summer day.

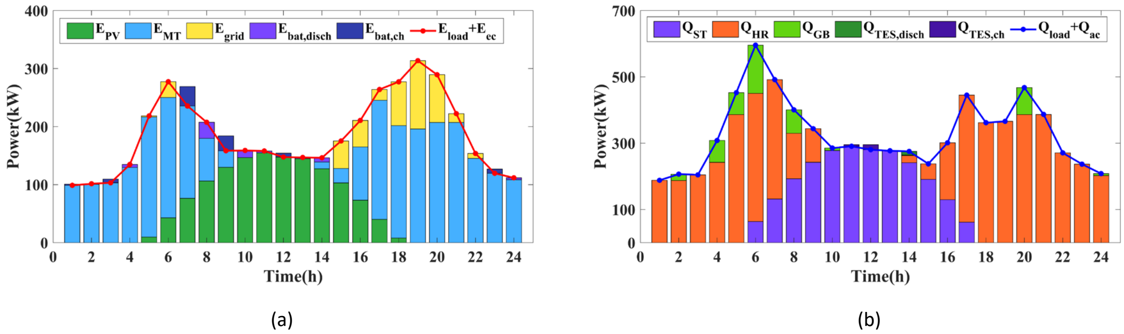

Fig 9. FB energy balance in a representative summer day.

Figure 7(a), during the period from 1:00 to 4:00, MT of the hybrid system under the FEL strategy bears the electricity demand of customers, during the period from 5:00 to 18:00, PV and MT generation bear most of the electricity demand of customers, and during the period from 19:00 to 24:00, MT bears most of the electricity demand, and a small amount of customer electricity demand is borne by the grid. Figure 8(a), during the period 1:00 to 4:00, MT of the hybrid system under the FTL strategy undertakes the all power demand of the customers, yet there is a small amount of power redundancy and power waste, during the period 5:00 to 18:00, the PV and MT generation undertakes most of the power demand of the customers, yet there is power redundancy and waste, and during the period 19:00 to 24:00, the MT takes up most of the electricity demand, and a small amount of customer electricity demand is taken up by the grid, a small amount of electricity redundancy and waste still exists. Figure 9(a), the battery under the proposed strategy starts charging when there is electrical energy redundancy in the hybrid system and can discharge in time when there is insufficient power generation in the hybrid system. Therefore, the hybrid system under the proposed strategy has no power redundancy and waste.

Figure 7(b), MT and GB undertake the thermal energy demand of users from 0:00 to 5:00, ST and MT undertake most of the thermal energy demand of users from 6:00 to 17:00, there is some thermal energy redundancy, and MT and GB undertake all the thermal energy demand of users from 18:00 to 24:00, there is some thermal energy redundancy and waste. Figure 8(b), MT and GB bear the thermal energy demand of customers from 0:00 to 5:00, ST and MT bear most of the thermal energy demand of customers from 6:00 to 17:00, and MT and GB undertake all the thermal energy demand of customers from 18:00 to 24:00. As shown in Figure 9(b), the TES can start absorbing heat when the system has electrical energy redundancy and release heat in time when the system is not producing enough heat. Therefore, the hybrid system under the proposed strategy does not have thermal redundancy and waste.

To sum up, the system generates electrical energy and thermal energy wastage under FTL and FEL strategies, respectively. The system operates under the proposed FB strategy and switches the operation strategy according to the energy storage state of the battery, which results in the elimination of the thermal energy waste under the FEL strategy and the electrical energy waste under the FTL strategy, respectively.

5.3.2. Analysis of operation in a representative transition season day

The operation of the system during a typical transition season day is as follows:

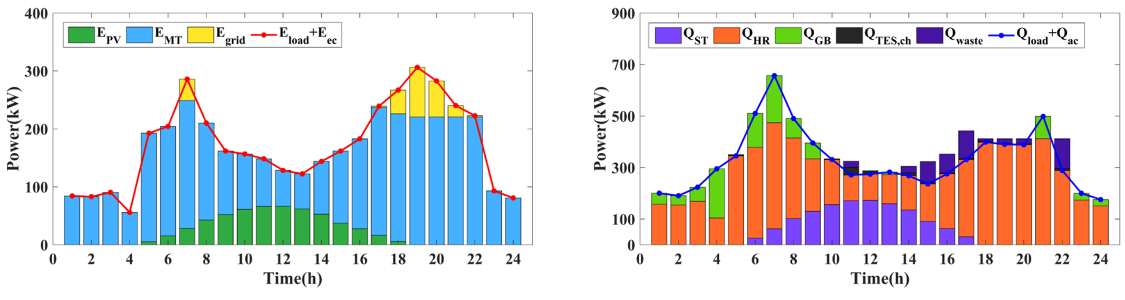

(a) (b)

Fig 10. FEL energy balance in a representative transition season day.

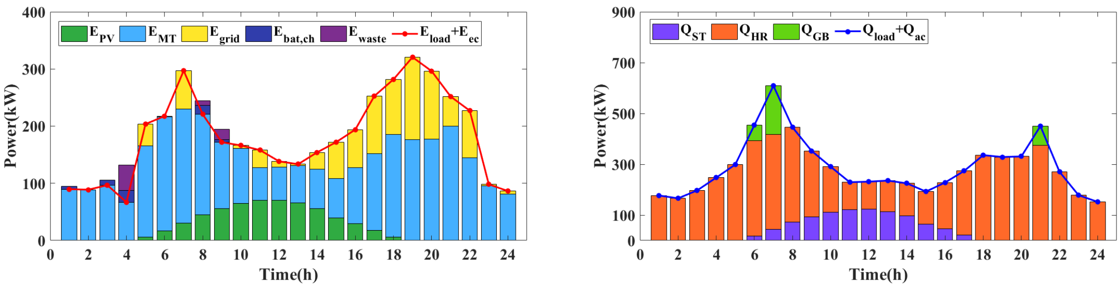

(a) (b)

Fig 11. FTL energy balance in a representative transition season day.

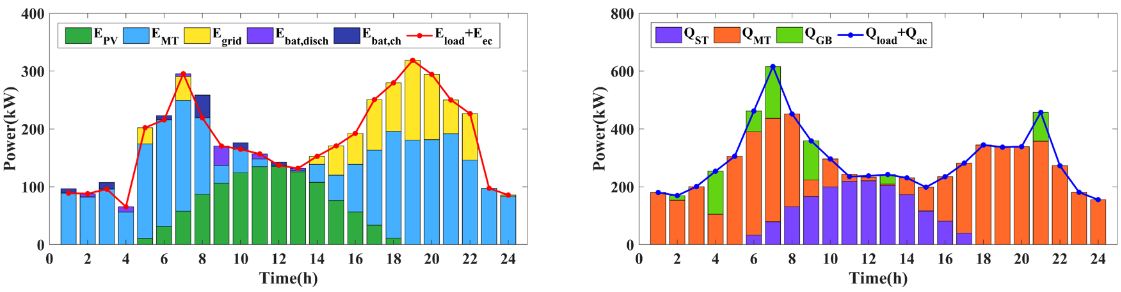

(a) (b)

Fig 12. FB energy balance in a representative transition season day.

Figure 10(a), 11(a), and 12(a), the power balance diagram indicates that the system under the FTL and FEL strategies is supplied with the majority of power by the MT for the customer, the PV starts to provide power to customers when the light intensity reaches a certain condition. When the electricity demand of users exceeds the generation capacity of the system, electricity is purchased from the grid to supplement this deficiency. The battery under the proposed strategy can absorb excess power and discharge it in time when the system is not generating enough power, thus eliminating power redundancy and waste.

Figure 10(b), 11(b), and 12(b), the system has thermal redundancy and waste when it runs under the FEL strategy, and the system can reliably bear the thermal energy demand of users when it runs the FTL strategy; for the system running under the FB strategy, the excess heat in the system is absorbed by the TES, and the thermal energy stored in the TES is released in time, and the proposed FB strategy does not cause thermal redundancy and thermal energy waste in the system compared with the FEL strategy.

In summary, a hybrid system operating under all three strategies can provide a reliable energy supply to the user. However, there is thermal energy redundancy and thermal energy waste under the FEL strategy, and there is electric energy redundancy and electric energy waste under the FTL strategy. The proposed strategy eliminates energy redundancy and waste by switching the strategy according to the battery storage state.

5.3.3. Analysis of operation in a representative winter day

The operation of the system during a typical winter day is as follows:

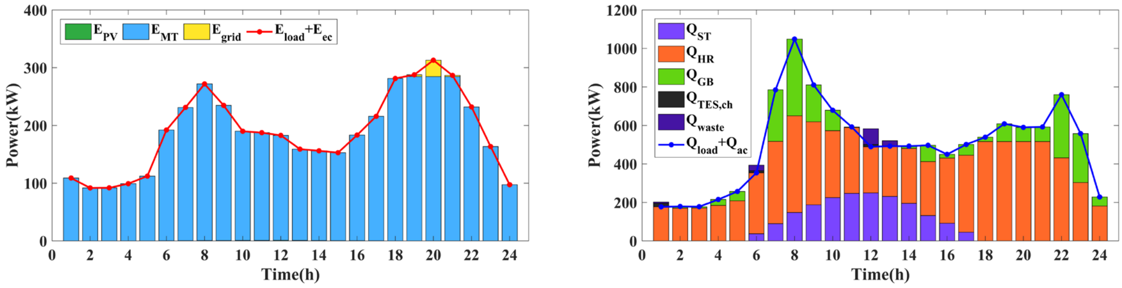

(a) (b)

Fig 13. FEL energy balance in a representative winter day.

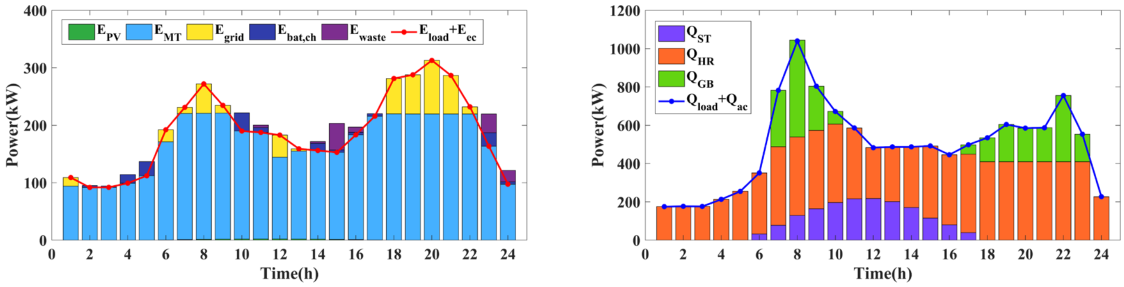

(a) (b)

Fig 14. FTL energy balance in a representative winter day.

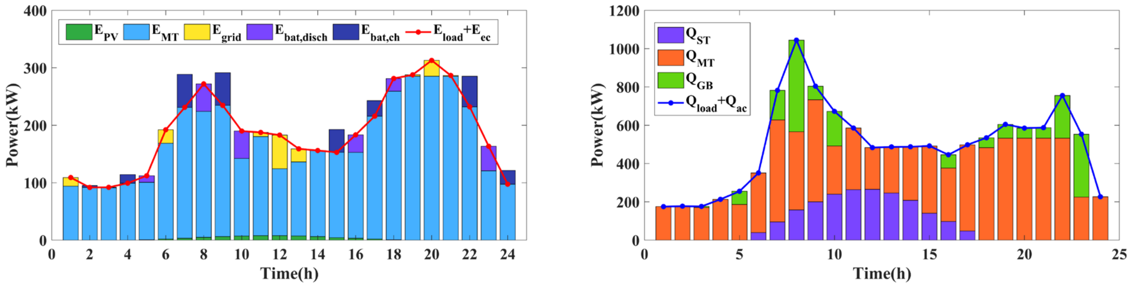

(a) (b)

Fig 15. FB energy balance in a representative winter day.

Figure 13, 14, and 15, the hybrid system under the FEL strategy can reliably meet the electrical energy demand of the users. When the system is running under the FTL strategy, the power demand of users is mainly provided by the MT, and when the hybrid system does not generate enough power to meet the users' demand, the grid will supply a portion of the electricity to users. However, the hybrid system under the FTL strategy has power redundancy and waste. The proposed strategy allows the system to switch between the two basic strategies according to the state of the battery storage, thus eliminating the redundancy and waste of power under the FTL strategy.

Figure 13, 14, and 15, the hybrid system under the FEL strategy can reliably meet the electrical energy demand of the users. When the system is running under the FTL strategy, the power demand of users is mainly provided by the MT, when the hybrid system does not generate enough power to meet the users, the grid supplies a portion of the electricity to users. However, the hybrid system under the FTL strategy has power redundancy and waste. The proposed strategy allows the system to switch between the two basic strategies according to the state of the battery storage, thus eliminating the redundancy and waste of power under the FTL strategy.

The above analysis indicated that the solar hybrid CCHP system constructed in this study achieved better environmental and energy performance in comparison to the conventional

CCHP system. In addition, the proposed operating strategy results in a hybrid system with better environmental and energy performance and eliminates energy redundancy and waste compared to the FTL and FEL operating strategies, thus improving the efficiency of the system, which facilitates better design and evaluation of hybrid CCHP systems.

6. Concluding Remarks

Coupling solar technologies into traditional combined cooling, heating, and power system is widely recognized as an effective way to solve energy-related problems. Therefore, this study establishes a mathematical model of a hybrid combined cooling, heating, and power system consisting of solar thermal and solar power technologies and proposes a novel operating strategy. In addition, the configuration of the hybrid system is optimized by a multi-objective arithmetic optimization algorithm. The findings contain the following sections:

- A multi-objective arithmetic optimization algorithm is developed by introducing mutation strategies, external archive mechanisms, and a non-dominated sorting strategy into the arithmetic optimization algorithm.
- The performance of the multi-objective arithmetic optimization algorithm is verified using a series of test functions.
- Considering Photovoltaic power and solar thermal technologies, a mathematical model of the hybrid combined cooling, heating, and power system is established. And a strategy to follow the energy storage state of the battery is proposed based on traditional operation strategies.
- The developed algorithm is used to optimize the configuration of hybrid systems under different operating strategies. The values of efficiency, boiler energy saving ratio, carbon

dioxide emission reduction ratio, and primary energy saving ratio indicators for the hybrid system under the proposed strategy are 78.51%, 88.26%, 54.64%, and 46.56%, respectively. These indicate that the hybrid system under the proposed strategy has significant effectiveness in improving system efficiency, reducing carbon dioxide emissions, and reducing primary energy consumption.

The contributions of this study are as follows: (1) Considering the equation constraint, capacity constraint, and climbing constraint, a mathematical model of a hybrid system is established; (2) A novel operation strategy is proposed, a novel multi-objective optimization approach is proposed to solve hybrid system configuration problem; (3) The distribution of the obtained Pareto optimal solution set is uniform, this proves the effectiveness of the proposed multi-objective arithmetic optimization algorithm in multi-objective optimization problems. Moreover, the research results contribute to improving the environmental performance and energy performance of the hybrid combined cooling, heating, and power system

The proposed algorithm achieved satisfactory results for the optimization of the hybrid system. Moreover, the proposed hybrid strategy improves the energy and environmental performance of the system. Future research needs to focus on applying the combined cooling, heating, and power system to other commercial buildings, and introducing other new energy sources into the combined cooling, heating, and power system.

Acknowledgements

This study was supported by the key project of Tianjin Natural Science Foundation [Project No. 19JCZDJC32100] and the Natural Science Foundation of Hebei Province of China [Project No. E2018202282].

References

[1] Mahian O, Mirzaie MR, Kasaeian A, Mousavi SH. Exergy analysis in combined heat and power systems: A review. *Energy Conversion and Management.* 2020;226. https://doi.org/10.1016/j.enconman.2020.113467.

[2] Rong A, Su Y. Polygeneration systems in buildings: A survey on optimization approaches. *Energy and Buildings.* 2017;151:439-454. https://doi.org/10.1016/j.enbuild.2017.06.077.

[3] Bandaru SH, Becerra V, Khanna S, Radulovic J, Hutchinson D, Khusainov R. A Review of Photovoltaic Thermal (PVT) Technology for Residential Applications: Performance Indicators, Progress, and Opportunities. *Energies.* 2021;14(13). https://doi.org/10.3390/en14133853.

[4] Li Y, Wang C, Li G, Chen C. Optimal scheduling of integrated demand response-enabled integrated energy systems with uncertain renewable generations: A Stackelberg game approach. *Energy Conversion and Management.* 2021;235. https://doi.org/10.1016/j.enconman.2021.113996.

[5] Li Y, Tian R, Wei M, Xu F, Zheng S, Song P, Yang B. An improved operation strategy for CCHP system based on high-speed railways station case study. *Energy Conversion and Management.* 2020;216. 10.1016/j.enconman.2020.112936.

[6] Kasaeian A, Bellos E, Shamaeizadeh A, Tzivanidis C. Solar-driven polygeneration systems: Recent progress and outlook. *Applied Energy.* 2020;264.

https://doi.org/10.1016/j.apenergy.2020.114764.

[7] Yang G, Zhai XQ. Optimal design and performance analysis of solar hybrid CCHP system considering influence of building type and climate condition. *Energy.* 2019;174:647-663. https://doi.org/10.1016/j.energy.2019.03.001.

[8] Fragiacomo P, Lucarelli G, Genovese M, Florio G. Multi-objective optimization model for fuel cell-based poly-generation energy systems. *Energy.* 2021;237. https://doi.org/10.1016/j.energy.2021.121823.

[9] Ai T, Chen H, Jia J, Song Y, Zhong F, Yang S, Xue G. Thermodynamic analysis of a CCHP system integrated with a regenerative organic flash cycle. *Applied Thermal Engineering.* 2022;202. https://doi.org/10.1016/j.applthermaleng.2021.117833.

[10] Nami H, Anvari-Moghaddam A, Nemati A. Modeling and analysis of a solar boosted biomass-driven combined cooling, heating and power plant for domestic applications. *Sustainable Energy Technologies and Assessments.* 2021;47. https://doi.org/10.1016/j.seta.2021.101326.

[11] Han Z, Wang J, Cui Z, Lu C, Qi X. Multi-objective optimization and exergoeconomic analysis for a novel full-spectrum solar-assisted methanol combined cooling, heating, and power system. *Energy.* 2021;237. https://doi.org/10.1016/j.energy.2021.121537.

[12] Mehregan M, Abbasi M, Khalilian P, Hashemian SM, Madadi A. Energy, economic, environmental investigations and optimization of a combined cooling, heating and power system with hybrid prime mover of gas engine and flat plate solar collector. *Energy Conversion and Management.* 2022;251.

https://doi.org/10.1016/j.enconman.2021.115018.

[13] Huang ZF, Wan YD, Soh KY, Chua KJ. Hybrid operating method to improve the part-load performance of gas turbine based combined cooling and power system. *Energy Conversion and Management.* 2020;226. https://doi.org/10.1016/j.enconman.2020.113506.

[14] Yang G, Zhai X. Optimization and performance analysis of solar hybrid CCHP systems under different operation strategies. *Applied Thermal Engineering.* 2018;133:327-340. https://doi.org/10.1016/j.applthermaleng.2018.01.046.

[15] Zheng CY, Wu JY, Zhai XQ. A novel operation strategy for CCHP systems based on minimum distance. *Applied Energy.* 2014;128:325-335. http://dx.doi.org/10.1016/j.apenergy.2014.04.084.

[16] Li L-L, Liu Y-W, Tseng M-L, Lin G-Q, Ali MH. Reducing environmental pollution and fuel consumption using optimization algorithm to develop combined cooling heating and power system operation strategies. *Journal of Cleaner Production.* 2020;247. https://doi.org/10.1016/j.jclepro.2019.119082.

[17] Wang J, Zhai Z, Jing Y, Zhang C. Particle swarm optimization for redundant building cooling heating and power system. *Applied Energy.* 2010;87(12):3668-3679. https://doi.org/10.1016/j.apenergy.2010.06.021.

[18] Jayasekara S, Halgamuge SK, Attalage RA, Rajarathne R. Optimum sizing and tracking of combined cooling heating and power systems for bulk energy consumers. *Applied Energy.* 2014;118:124-134. https://doi.org/10.1016/j.apenergy.2013.12.040.

[19] Liu Z-F, Li L-L, Liu Y-W, Liu J-Q, Li H-Y, Shen Q. Dynamic economic emission dispatch considering renewable energy generation: A novel multi-objective optimization approach. *Energy.* 2021;235. https://doi.org/10.1016/j.energy.2021.121407.

[20] Li L-L, Liu Z-F, Tseng M-L, Zheng S-J, Lim MK. Improved tunicate swarm algorithm: Solving the dynamic economic emission dispatch problems. *Applied Soft Computing.* 2021;108. https://doi.org/10.1016/j.asoc.2021.107504.

[21] Wang J-J, Jing Y-Y, Zhang C-F. Optimization of capacity and operation for CCHP system by genetic algorithm. *Applied Energy.* 2010;87(4):1325-1335. https://doi.org/10.1016/j.apenergy.2009.08.005.

[22] Barbieri ES, Dai YJ, Morini M, Pinelli M, Spina PR, Sun P, Wang RZ. Optimal sizing of a multi-source energy plant for power heat and cooling generation. *Applied Thermal Engineering.* 2014;71(2):736-750. https://doi.org/10.1016/j.applthermaleng.2013.11.022.

[23] Ismail MS, Moghavvemi M, Mahlia TMI. Genetic algorithm based optimization on modeling and design of hybrid renewable energy systems. *Energy Conversion and Management.* 2014;85:120-130. https://doi.org/10.1016/j.enconman.2014.05.064.

[24] Zhang J, Cao S, Yu L, Zhou Y. Comparison of combined cooling, heating and power (CCHP) systems with different cooling modes based on energetic, environmental and economic criteria. *Energy Conversion and Management.* 2018;160:60-73. https://doi.org/10.1016/j.enconman.2018.01.019.

[25] Chen K, Pan M. Operation optimization of combined cooling, heating, and power

superstructure system for satisfying demand fluctuation. *Energy.* 2021;237. https://doi.org/10.1016/j.energy.2021.121599.

[26] Wang J, Zhou Y, Zhang X, Ma Z, Gao Y, Liu B, Qin Y. Robust multi-objective optimization with life cycle assessment of hybrid solar combined cooling, heating and power system. *Energy Conversion and Management.* 2021;232. https://doi.org/10.1016/j.enconman.2021.113868.

[27] Guo L, Liu W, Cai J, Hong B, Wang C. A two-stage optimal planning and design method for combined cooling, heat and power microgrid system. *Energy Conversion and Management.* 2013;74:433-445. https://doi.org/10.1016/j.enconman.2013.06.051.

[28] Ma T, Wu J, Hao L, Lee W-J, Yan H, Li D. The optimal structure planning and energy management strategies of smart multi energy systems. *Energy.* 2018;160:122-141. https://doi.org/10.1016/j.energy.2018.06.198.

[29] Wu N, Zhan X, Zhu X, Zhang Z, Lin J, Xie S, Meng C, Cao L, Wang X, Shah N, Zheng X, Zhao Y. Analysis of biomass polygeneration integrated energy system based on a mixed-integer nonlinear programming optimization method. *Journal of Cleaner Production.* 2020;271. https://doi.org/10.1016/j.jclepro.2020.122761.

[30] Facci AL, Andreassi L, Ubertini S. Optimization of CHCP (combined heat power and cooling) systems operation strategy using dynamic programming. *Energy.* 2014;66:387-400. https://doi.org/10.1016/j.energy.2013.12.069.

[31] Li C, Zhou J, Ouyang S, Ding X, Chen L. Improved decomposition-coordination and discrete differential dynamic programming for optimization of large-scale hydropower

system. *Energy Conversion and Management.* 2014;84:363-373. https://doi.org/10.1016/j.enconman.2014.04.065.

[32] Ikeda S, Ooka R. Metaheuristic optimization methods for a comprehensive operating schedule of battery, thermal energy storage, and heat source in a building energy system. *Applied Energy.* 2015;151:192-205. https://doi.org/10.1016/j.apenergy.2015.04.029.

[33] Wang J, Liu Y, Ren F, Lu S. Multi-objective optimization and selection of hybrid combined cooling, heating and power systems considering operational flexibility. *Energy.* 2020;197. https://doi.org/10.1016/j.energy.2020.117313.

[34] Zeng R, Li H, Liu L, Zhang X, Zhang G. A novel method based on multi-population genetic algorithm for CCHP-GSHP coupling system optimization. *Energy Conversion and Management.* 2015;105:1138-1148. https://doi.org/10.1016/j.enconman.2015.08.057.

[35] Hou H, Wu J, Ding Z, Yang B, Hu E. Performance analysis of a solar-assisted combined cooling, heating and power system with an improved operation strategy. *Energy.* 2021;227. https://doi.org/10.1016/j.energy.2021.120516.

[36] Zhang T, Yang C, Chen H, Sun L, Deng K. Multi-objective optimization operation of the green energy island based on Hammersley sequence sampling. *Energy Conversion and Management.* 2020;204. https://doi.org/10.1016/j.enconman.2019.112316.

[37] Wei D, Chen A, Sun B, Zhang C. Multi-objective optimal operation and energy coupling analysis of combined cooling and heating system. *Energy.* 2016;98:296-307.

https://doi.org/10.1016/j.energy.2016.01.027.

[38] Tan B, Chen H. Stochastic Multi-Objective Optimized Dispatch of Combined Cooling, Heating, and Power Microgrids Based on Hybrid Evolutionary Optimization Algorithm. *Ieee Access.* 2019;7:176218-176232. https://doi.org/10.1109/ACCESS.2019.2955515.

[39] Ehyaei MA, Ahmadi A, Assad MEH, Rosen MA. Investigation of an integrated system combining an Organic Rankine Cycle and absorption chiller driven by geothermal energy: Energy, exergy, and economic analyses and optimization. *Journal of Cleaner Production.* 2020;258. https://doi.org/10.1016/j.jclepro.2020.120780.

[40] Yao E, Wang H, Wang L, Xi G, Marechal F. Multi-objective optimization and exergoeconomic analysis of a combined cooling, heating and power based compressed air energy storage system. *Energy Conversion and Management.* 2017;138:199-209. https://doi.org/10.1016/j.enconman.2017.01.071.

[41] Wang H, Zhang R, Peng J, Wang G, Liu Y, Jiang H, Liu W. GPNBI-inspired MOSFA for Pareto operation optimization of integrated energy system. *Energy Conversion and Management.* 2017;151:524-537. https://doi.org/10.1016/j.enconman.2017.09.005.

[42] Boyaghchi FA, Chavoshi M. Monthly assessments of exergetic, economic and environmental criteria optimization of a solar micro-CCHP based on DORC. *Solar Energy.* 2018;166:351-370. https://doi.org/10.1016/j.solener.2018.03.069.

[43] Cao Y, Rad HN, Jamali DH, Hashemian N, Ghasemi A. A novel multi-objective spiral optimization algorithm for an innovative solar/biomass-based multi-generation energy system: 3E analyses, and optimization algorithms comparison. *Energy*

Conversion and Management. 2020;219. https://doi.org/10.1016/j.enconman.2020.112961.

[44] Behzadian M, Otaghsara SK, Yazdani M, Ignatius J. A state-of the-art survey of TOPSIS applications. *Expert Systems with Applications.* 2012;39(17):13051-13069. https://doi.org/10.1016/j.eswa.2012.05.056.

[45] EN 12975-2:2006, Thermal solar systems and components – Solar collectors – Part2: Test methods. Beuth Verlag, Berlin, 2006.

[46] Li L-L, Zheng S-J, Tseng M-L, Liu Y-W. Performance assessment of combined cooling, heating and power system operation strategy based on multi-objective seagull optimization algorithm. *Energy Conversion and Management.* 2021;244. https://doi.org/10.1016/j.enconman.2021.114443.

[47] Ren FK, Wang JJ, Zhu ST, Chen Y. Multi-objective optimization of combined cooling, heating and power system integrated with solar and geothermal energies. *Energy Conversion and Management.* 2019;197:14. https://doi.org/10.1016/j.enconman.2019.111866.

[48] Abualigah L, Diabat A, Mirjalili S, Elaziz MA, Gandomi AH. The Arithmetic Optimization Algorithm. *Computer Methods in Applied Mechanics and Engineering.* 2021;376. https://doi.org/10.1016/j.cma.2020.113609.

[49] Nebro AJ, Durillo JJ, Garcia-Nieto J, Coello CAC, Luna F, Alba E, Ieee. SMPSO: A New PSO-based Metaheuristic for Multi-objective Optimization. Paper presented at: IEEE Symposium on Computational Intelligence in Multi-Criteria Decision-Making; Mar

30-Apr 02, 2009; Nashville, TN. https://doi.org/10.1109/MCDM.2009.4938830

[50] Miao FH, Yao L, Zhao XJ. Symbiotic organisms search algorithm using random walk and adaptive Cauchy mutation on the feature selection of sleep staging. Expert Systems with Applications. 2021;176:17. https://doi.org/10.1016/j.eswa.2021.114887.

[51] E. Zitzler, K. Deb, L. Thiele, Comparison of multiobjective evolutionary algorithms: empirical results., Evol. Comput. 8 (2) (2000) 173–195, https://dx.doi.org/10.1162/106365600568202.

[52] Coello, C. A. C., & Lamont, G. B. (2004). Applications of multi-objective evolutionary algorithms: Vol. 1. World Scientific.

[53] Schott, J. R. (1995). Fault tolerant design using single and multicriteria genetic algorithm optimization: DTIC document. Massachusetts Institute of Technology, Department of Aeronautics and Astronautics.

[54] Deru M, Field K, Studer D. U.S. Department of Energy Commercial Reference Building Models of the National Building Stock, https://www.energy.gov/eere/buildings/commercial-reference-buildings; 2011 [Accessed 9 September 2020].

[55] Wilson E. Commercial and Residential Hourly Load Profiles for all TMY3 Locations in the United States, https://openei.org/doe-opendata/dataset/commercial-and-residential-hourly-load-profiles-for-all-tmy3-locations-in-the-united-states; 2020 [Accessed 9 September 2020].

[56] Wang J, Yang Y. Energy, exergy and environmental analysis of a hybrid combined cooling heating and power system utilizing biomass and solar energy. Energy Conversion and Management. 2016;124:566-577. https://doi.org/10.1016/j.enconman.2016.07.059.

[57] Liu, Y.W., Li, L.L., Tseng, ML., Lim, MK. & Ali, MH. Optimal scheduling of combined cooling, heating, and power microgrid based on a hybrid gray wolf optimizer, Journal of Industrial and Production Engineering. 2021; DOI: 10.1080/21681015.2021.1974963